Data-Driven Soil Water Content Estimation at Multiple Depths Using SFCW GPR

Vincent Filardi[†*] Worcester, MA, USA vfilardi@wpi.edu

Allen Cheung[†*] Worcester, MA, USA acheung@wpi.edu

Ruba Khan[†*] Worcester, MA, USA rkhan@wpi.edu

Oren Mangoubi[†*‡] Worcester, MA, USA omangoubi@wpi.edu

Majid Moradikia[†§] Worcester, MA, USA mmoradikia@wpi.edu

Seyed (Reza) Zekavat[†*§] Worcester, MA, USA rezaz@wpi.edu

Brian Wilson[†‖] Ann Arbor, Michigan, USA brwilson@mtu.edu

Radwin Askari[ǂ¶] Ann Arbor, Michigan, USA raskari@mtu.edu

Douglas Petkie[†§] Worcester, MA, USA brwilson@mtu.edu

***Abstract*—This paper provides a cost-effective solution to Soil Water Content (SWC) estimation at multiple root-zone depths using Ground Penetrating Radar (GPR) and Machine Learning (ML) based on an extensive measurement campaign conducted at Worcester Polytechnic Institute (WPI). SWC characterization is critical for optimal industrial farming irrigation and, in turn, impacts water conservation and the mitigation of soil quality degradation. Accurate prediction of the water table and SWC of the root-zone soil is invaluable for precision farming. High-resolution modeling of SWC at varying sub-surface depths can potentially increase irrigation efficiency and the yield of crops such as maize, which has a massive water footprint upwards of 768 billion cubic meters and accounts for an estimated 5% percent of the world's daily calorie intake. Traditional methods of subsurface soil characterization by subsurface probes are invasive, costly, and labor-intensive. Our approach generates an accurate and precise characterization of the soil water content of loamy soil at multiple root level depths using Signal Processing principles and ML applied to a small dataset of size 51 of real field measurements collected between October 20th to 30th 2022. We applied ML algorithms to the preprocessed data collected by a Stepped Frequency Continuous Wave (SFCW) GPR signal and extracted the most relevant features related to SWC prediction at multiple depths. We used these extracted features to achieve a mean absolute percentage error as low as 6% across the four root-zone depths of our field data. This study was conducted within the 0.4 to 2.0 GHz frequency range, and provides an analysis of frequencies key to root-zone SWC characterization.**

***Index Terms*—Ground Penetrating Radar, Soil Water Content, Machine Learning**

I. Introduction

As population growth continues, protecting soil quality comes into prominence for our global ecosystem [1]–[4]. Nowadays, farmers have a key role in reducing land damage and boosting food supply by using the right amount of water for irrigation [5]. But, to do this effectively, we need to know and keep track of soil conditions. Particularly, accurate estimation of the Soil Water Content (SWC) can solve many challenges in farming and help protect our environment [6]–[8]. Sensors can be used to measure the water content of the soil or the soil's permittivity to estimate this water content [9]. However, these methods can be too costly for large farms due to the expense of buying, installing, and maintaining such sensors. This problem affects farming at all levels, so we need different methods to monitor soil health and make precision farming possible.

Recently, Ground Penetrating Radar (GPR) has gained interest as an effective non-invasive tool capable of capturing subsurface features, saving time and money compared to physical measurement tools [10]. GPR has found many use-cases, like detecting underground objects [11]–[14], identifying threats [15]–[18], and specifically, estimating soil moisture [19]–[27]. The unique and inhomogeneous composition of the soil can greatly influence its electrical properties, which in turn shape the reflected GPR signal in terms of speed, attenuation, delay of propagation, and signal loss in certain frequencies [28], [29]. Among these properties, soil moisture is of great importance as it affects both the permittivity and conductivity of the soil [30], [31]. Notably, the permittivity of water is 27 times higher than that of common soil minerals, leading to a more pronounced attenuation of the GPR signal [32]. This factor highlights the need to carefully select the frequency range [23], [33] which impacts the ability of GPR to characterize SWC. To deal with this concern, for this study, we selected a wide-band Stepped Frequency Continuous Wave (SFCW) GPR system to collect data. Our goal was to have a high resolution in the frequency domain and to enhance the Signal-to-Noise Ratio (SNR), providing more accurate and reliable readings [34].

A piece of research focusing on GPR-based SWC estimation, utilizes either synthetic data [35] or data from controlled laboratory environments [21], [36], [37]. In contrast, the data for our study was collected during a measurement campaign from 10/19/2022 to 10/23/2022 and 10/29/2022 to 10/30/2022, in Worcester, Massachusetts, in collaboration with Worcester Polytechnic Institute (WPI) and Michigan Tech Research Institute (MTRI). In the field, many studies apply

† Worcester Polytechnic Institute
† Michigan Tech Research Institute
ǂ Michigan Tech University
* Data Science
§ Physics
‡ Mathematical Sciences
¶ Geological and Mining Engineering and Sciences
‖ Research Engineer

a technique that measures the flight time of a radar signal reflected off markers set at specified depths. This information is used to derive the SWC, based on the principle that the radar signal's velocity varies with the soil's water content [20], [25], [38]–[40]. However, our research takes a different approach. This approach is more complex but more reflective of real-world agricultural conditions, where precise depth markers may not be available. Thus, our method provides a practical solution for estimating SWC in real-world farming contexts. In addition, while some studies take a physics-based approach to characterize the dielectric properties of soil and SWC [41]–[43], they may not suit real-world scenarios. With increasing uncertainty of the heterogeneous subsurface, the number of unknown parameters rises, resulting in a higher computational cost to solve the ill-posed problem [44]. Additionally, the solution must be recomputed every time SWC needs to be estimated on a new soil patch. To circumvent these challenges, we employ a data-driven supervised learning to characterize SWC. While many studies use data-driven approaches for estimating SWC, few have considered measuring SWC at different depths in the root-zone [19], [22], [45]–[48]. Our research seeks to fill this gap by focusing on layered SWC estimation. The goal is to create a detailed map of root-zone soil moisture for more precise irrigation practices in industrial farming. Building on the work of [23], [33], we also aim to identify the frequency range that provides the most useful information for SWC estimation, using Machine Learning (ML) algorithms that consider feature importance.

Based on the preceding discussion, the key contributions of our research are:

- We present a data-driven method for predicting SWC at multiple root-zone depths, particularly suited to scenarios with limited data.
- Our approach leverages computationally efficient ML algorithms. To be specific, we utilize Leave-One-Out Cross Validation with our ML algorithms, enabling reliable SWC estimation across four root-zone depths even with low quantities of data.
- We identify the optimal frequency ranges for future SWC estimation using SFCW GPR, enhancing the practical utility of our method.
- All data used in this study (51 data points in total) are real and were collected during a measurement campaign.

Outline of paper: In Section II we provide an overview of the SFCW GPR transmission scheme and the supervised learning framework used, followed by a short discussion of our data campaign and data preprocessing methods in Section III. In Section IV we discuss our data analysis methods. In Section V we show the results of our analysis and discuss feature importance. We discuss conclusions and future directions in Section VI.

II. Preliminaries and Discussion

In this study, we analyzed backscattered GPR data from loam soil to estimate SWC at different depths. The GPR system used an SFCW transmission waveform. For the prediction of SWC, we formulated this task as a supervised learning problem and employed ML algorithms on our collected GPR data. In what follows, we will first provide a quick overview of the necessary concepts and then present our research work.

Stepped Frequency Continuous Wave Radar: The limitations of a standard pulsed radar include potential restrictions in power and bandwidth. For this reason, we used a GPR capable of transmitting and receiving wideband SFCW. With a chosen frequency interval Δf, the SFCW emits a waveform over N discrete uniformly spaced pulses every Δt s over bandwidth $B = N\Delta f$. We can define the n^{th} pulse of the SFCW, transmitted at time t_n, with a carrier frequency f_c as follows:

$$s_n(t_n) = e^{j2\pi(f_n t_n)} \quad f_n = f_c + (n-1)\Delta f.$$

The duration of one entire sweep of the SFCW radar can be calculated by $T = N\Delta t$.

For each transmitted pulse, the in-phase (real component) and quadrature (imaginary component) samples in the frequency domain were measured by the receiver to calculate the phase shift between the received pulse and reference signal for each frequency. For each measurement i, we represent a sweep of the SFCW as the complex-valued vector $\mathbf{S}_i$:

$$\mathbf{S}_i = [s_1, s_2, \ldots, s_N].$$

In this work, we chose not to utilize additional processing such as inverse discrete Fourier transform, typically used to resolve the subsurface range profile [49]. The reason for this choice is that the stepped frequency radar, used in our application, inherently provides a high-frequency resolution sufficient for SWC estimation. The SFCW's advantage lies in its high-resolution capabilities in the frequency domain. The high frequency resolution of SFCW facilitates a detailed study of the interactions between the soil channel and radar signals across a broad bandwidth. Moreover, the SFCW radar's intrinsic nature effectively minimizes any radio frequency interference. Thus, our method's design sidesteps the need for additional pre-processing often used to refine the subsurface range profile.

Supervised Learning Framework: We consider the inverse medium problem of predicting the root-zone SWC of a loam patch from observed SFCW radar signals backscattered off the different sub-layers. We adopt a data-driven approach to this problem by formulating it as a supervised learning problem. Like other supervised learning tasks, we utilize a dataset $D = \{x_i, y_i\}^n$ of size n that includes predictor variables x_i and labels y_i. For our particular problem, the predictor variables x_i are complex-valued received backscattered SFCW sweeps $\mathbf{S}_i$ for each experiment i. The labels y_i are continuous-valued vectors of size four, representing SWC at four different depths for the corresponding experiment i. Our goal is to predict the dependent variables y_i using the observed independent features x_i from our dataset D. We formulate this as

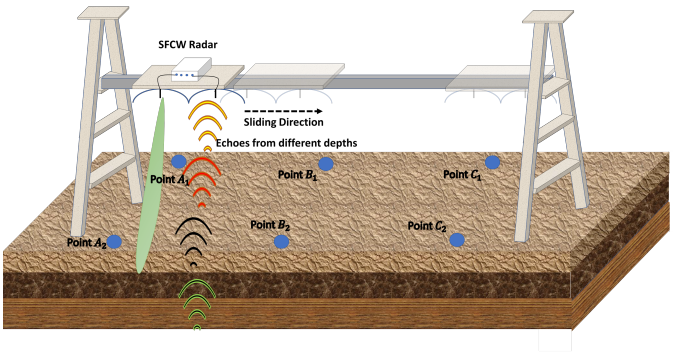

Fig. 1: Measurement campaign setup at WPI. A rail, holding the SFCW GPR, is placed between two ladders, with the GPR centrally positioned above two horizontal probe lines. Measurements were taken at 34, 57, and 79 inches above the ground. For each probe A_1, A_2, B_1, B_2, C_1, and C_2, SWC was recorded at 10, 20, 30, and 40 cm depths.

a minimization problem, searching for a ML model $\hat{g}$ with trainable parameters θ:

$$\min_{\theta} \sum_{i=1}^{n} \ell\left(\hat{g}(x_i, \theta), y_i\right) \tag{1}$$

where the loss function ℓ quantifies the error of the prediction $\hat{g}(x_i, \theta)$ of the label y_i for each datapoint x_i. We denote the optimal trainable θ parameters, which minimize (1), by $\theta^{\star}$.

III. Measurement and Data Preprocessing

Our experiment data were collected during our 2022 measurement campaign at WPI, spanning from October 19th to 23rd and 29th to 30th. We used an off-the-shelf Akela radar [50] equipped with log-periotic antennas, range gating, a low-noise amplifier, and an SFCW transmission scheme. We selected 4096 uniformly spaced frequencies within the 0.4 to 2.0 GHz range for our SFCW bandwidth.

We placed the radar over a loam patch, as depicted in Fig. 1, with the rail positioned above six probes A_1, A_2, B_1, B_2, C_1, and C_2. The distance between probes A_1-A_2, B_1-B_2 and C_1-C_2 was 4 feet, while the distance between A_i-B_i and B_i-C_i (where $i = 1, 2$) was 2 feet.

As indicated in Fig. 1, the rail carrying the radar was centrally positioned along each horizontal line of probes. We took roughly 100 SFCW radar sweeps S_i (size 4096) at three heights (34 in, 57 in, 79 in) for each experiment i, while the radar was centered between one of the probes pairs A, B, or C. To improve the signal-to-noise ratio, we averaged the sweeps $S_1, S_2, \ldots, S_{100}$ for each height. Each height's average sweeps were then concatenated to form x_i of size 12288 (4096×3) for each experiment i.

Correspondingly, at each probe location A_1, A_2, B_1, B_2, C_1, and C_2, we used a Dynamax PR2/4 Soil Moisture probe [51] to record the soil moisture at depths of 10, 20, 30, and 40 cm for each probe. We averaged the recorded SWC accross each probe coupling at each depth, generating a vector y_i of size 4 for the designated probe couplings A, B, or C of an experiment. In total, we performed 17 successful measurements for each probe pair A, B, and C during the campaign, producing a dataset of size 51, $D = \{x_i, y_i\}^{51}$.

We found the best preprocessing method for the independent feature sx_i as follows: 1) concatenation of the real and imaginary components of each x_i resulting in a vector of size 24576 (12288×2), and 2) centering each feature x_i. This preprocessing method led to optimal supervised learning algorithm model performance because it preserves as much of the original information in the data as possible. We noticed that the downstream models $\hat{g}$ achieved a much higher performance when the variance of the independent features was preserved by just centering the data. Feature engineering methods that require a standard deviation of the independent features to be unit length one, such as Z-Score Transformation, Principal Component Analysis, and Kernel Principal Component Analysis, did not improve the performance across models. We believe this is because of the information lost in the variance after the data transformations.

IV. Proposed Data-Driven SWC Estimation

Let $\hat{g}$ represent our chosen ML model. In this study, we explored several $\hat{g}$ candidates, including Linear Regression (LR), Lasso Regression (Lasso), Random Forest (RF), and XGBoost (XGB). These model candidates were selected because they are traditional ML algorithms known for their interpretability, flexibility, and ability to handle small datasets effectively. Lasso was particularly chosen for its capability in sparse feature selection by its l_1 penalty term within its objective function. For each $\hat{g}$, we aimed to find the optimal model parameters $\theta^{\star}$ that minimized the loss function ℓ of Equation 1. For this paper, we choose ℓ to be the Root Mean Squared Error (RMSE) as defined:

$$RMSE(y, \hat{g}(x, \theta^{\star})) = \sqrt{\frac{1}{n} \sum_{i=1}^{n} \left(y_i - \hat{g}\left(x_i, \theta^{\star}\right)\right)^2}. \tag{2}$$

We also report the Mean Absolute Percentage Error (MAPE), as given by:

$$MAPE(y, \hat{g}(x, \theta^{\star})) = \frac{1}{n} \sum_{i=1}^{n} \left| \frac{y_i - \hat{g}(x_i, \theta^{\star})}{y_i} \right|. \tag{3}$$

For both equations, n is the number of data points, y_i is the SWC measurement for datapoint i measured by a subsurface probe at four depths, and $\hat{g}\left(x_i, \theta^{\star}\right)$ is the predicted values for the SWC for each depth using the GPR signal x_i for datapoint i.

Parameter Search and Validation: With a relatively small dataset of size 51, we did not feel that a traditional training/validation/test split was appropriate and took advantage of leave-one-out cross validation. We opted to tune our hyperparameters θ on all points but the left out point of leave one out

TABLE I: This table provides the training and test errors of the different ML methods, averaged over all depths for each ML model. The best observed performing model, Linear Regression, is highlighted in bold. The test results are averaged over the left out data point of leave-one-out cross validation with standard error.

Model	Train error	Test error	
	RMSE	RMSE	MAPE
Linear Regression	0 ±0	**1.65 ± 0.2**	**5.43% ± 0.7**
Lasso	0.005 ± 0	1.96 ±0.2	6.28% ±0.7
Random Forest	1.12 ±0	2.52 ±.5	8.42% ±0.6
XGBoost	0.62 ±0	2.39 ±0.2	8.0% ±1.0

TABLE II: This table gives the the test errors of the the best performing ML methods, per depth. The results are averaged over the left out data point of leave-one-out cross validation with standard error.

Depth	Best Model	Test error	
		RMSE	MAPE
10 cm	Linear Regression	1.83 ±0.25	7.28% ±1.01
20 cm	Linear Regression	1.78 ±0.23	6.12% ±0.85
30 cm	Linear Regression	1.95 ±0.25	6.14% ±0.84
40 cm	XGBoost	1.03 ±0.13	2.10% ±0.25

cross validation using 5-fold cross validation [52]. This was done to estimate the expected sample error for each model and determine the best hyperparameters $\theta^{\star}$ which generalize the best to unseen data. The average RMSE across all folds of the training stage and RMSE and MAPE of the testing stage on the left out datapoint are shown in Table I averaged across all four probe depths. Additional results are presented in Table II, which show the best performing model observed for each individual probe depth.

V. Results

Model Results We performed one experiment on our dataset, determining the best $\hat{g}$ with best parameters θ^{*} such that we minimize Equation 1. We considered 4 different models: Linear Regression (LR), Lasso, Random forest (RF), and XGBoost (XGB). The test RMSE and MAPE results can be seen for each model in Table I. The best parameters of each model were determined by the best performing θ for each fold of the leave-one-out cross validation. We observe the LR model performed the best averaged over all 4 depths with an test RMSE of 1.65 and a test MAPE of 5.43%. For a more detailed view of each individual probes, we highlight the best model for each depth in Table II. The test errors, measured in terms of RMSE and MAPE, are provided for each depth. The best model for all depths was LR except for the depth of 40 cm, where XGB was the best model. For depths of 10 cm, 20 cm, and 30 cm, the LR model achieved RMSE values of 1.83, 1.78, and 1.95, respectively, with corresponding MAPE values of 7.28%, 6.12%, and 6.14%. For the 40 cm probe, the XGB model performed the best at the depth of 40 cm, achieving an RMSE of 1.03 and a MAPE of 2.10%.

Feature Analysis In Fig. 2, we analyze the frequency importance of each depth using Lasso's sparse feature selection by its l_1 penalty on the coefficients. While RF and XGB both have a measure of feature importance, we show Lasso's because it performed better on average across depths as shown in Table I. Over 1050 model training stages, we plot the percentage of model fits where the coefficients of each feature are non-zero. Each subplot shows the importance of a feature for a specific depth, as labeled by each subplot title. The most important features selected by Lasso correspond to SFCW GPR frequencies (x-axis) with a higher percentage (y-axis) of non-zero coefficient values across the trials.

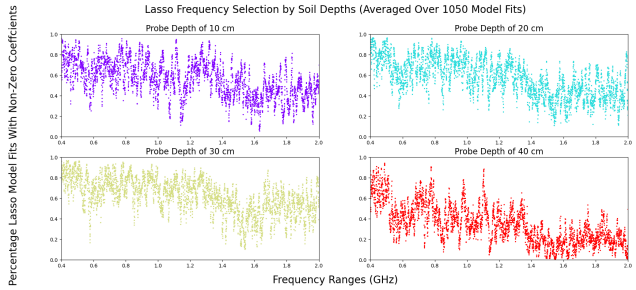

Fig. 2: Frequency analysis scatter plots by Lasso feature selection by depth over all 4096 SFCW frequencies. Percentage of trials with non zero coefficients across 1050 model training stages. We suggest to view the figure on a computer and zoomed in.

VI. Conclusion

In this study, we have shown that the problem of SWC estimation of field data can be effectively solved using a data-driven approach. With our preprocessing method, we show that even traditional ML algorithms, such as LR, Lasso, RF, and XGB, can achieve relatively low errors (between 7.28% and 2.10% MAPE) across multiple soil depths. We see in all plots of Fig. 2 by the varying percentages that frequencies close together do not necessarily provide additional information to Lasso and are set more often to zero coefficients. This suggests that our data campaign may have been able to get away with a smaller step size, N, for the SFCW. This change would result in faster data collection and reduce the complexity and computational cost of our SWC estimation models with fewer features. Notably, in the bottom-right subplot of 40 cm, Lasso set many of the higher frequency features to zero compared to the subplots of all other depths. This is expected because higher frequencies do not provide useful information for predicting SWC at lower depths owing to the higher degrees of attenuation and lack of penetration at depths. We find this very interesting, as it suggests that the model was able to capture some GPR backscatter behaviour with just the data. In addition to prescribing a longer data campaign, we also suggest a lower step size N for the SFCW GPR and a frequency range tailored for specific target depths for future work.

ACKNOWLEDGMENT

Oren Mangoubi and Vincent Filardi were supported by NSF CCF-2104528. Allen Cheung, Ruba Khan, Seyed Zekavat, Radwin Askari, Douglas Petkie, and Majid Moradikia were supported by USDA grant NR223A750013G032. All authors are particularly thankful for the involvement and support of Brian Wilson and all collaborators at MTRI.

REFERENCES

[1] B. J. Wienhold, S. Andrews, and D. Karlen, "Soil quality: a review of the science and experiences in the usa," *Environmental Geochemistry and Health*, vol. 26, pp. 89–95, 2004.

[2] C. S. Ferreira, S. Seifollahi-Aghmiuni, G. Destouni, N. Ghajarnia, and Z. Kalantari, "Soil degradation in the european mediterranean region: Processes, status and consequences," *Science of the Total Environment*, vol. 805, p. 150106, 2022.

[3] R. Zhao and K. Wu, "Soil health evaluation of farmland based on functional soil management—a case study of yixing city, jiangsu province, china," *Agriculture*, vol. 11, no. 7, p. 583, 2021.

[4] E. B. Jiru and H. T. Wegari, "Soil and water conservation practice effects on soil physicochemical properties and crop yield in ethiopia: review and synthesis," *Ecological Processes*, vol. 11, no. 1, pp. 1–16, 2022.

[5] M. M. Tahat, K. M. Alananbeh, Y. A. Othman, and D. I. Leskovar, "Soil health and sustainable agriculture," *Sustainability*, vol. 12, no. 12, p. 4859, 2020.

[6] A. L. Virk, M. A. Noor, S. Fiaz, S. Hussain, H. A. Hussain, M. Rehman, M. Ahsan, and W. Ma, "Smart farming: An overview," in *Smart Village Technology*, ser. Modeling and optimization in science and technologies. Cham: Springer International Publishing, 2020, pp. 191–201.

[7] S. D. Keesstra, J. Bouma, J. Wallinga, P. Tittonell, P. Smith, A. Cerdà, L. Montanarella, J. N. Quinton, Y. Pachepsky, W. H. Van Der Putten *et al.*, "The significance of soils and soil science towards realization of the united nations sustainable development goals," *Soil*, vol. 2, no. 2, pp. 111–128, 2016.

[8] S. Touil, A. Richa, M. Fizir, J. E. Argente Garcia, and A. F. Skarmeta Gomez, "A review on smart irrigation management strategies and their effect on water savings and crop yield," *Irrigation and Drainage*, 2022.

[9] G. C. Topp, J. Davis, and A. P. Annan, "Electromagnetic determination of soil water content: Measurements in coaxial transmission lines," *Water resources research*, vol. 16, no. 3, pp. 574–582, 1980.

[10] K. Zajícová and T. Chuman, "Application of ground penetrating radar methods in soil studies: A review," *Geoderma*, vol. 343, pp. 116–129, 2019.

[11] E. Aydin and S. E. Yüksel, "Buried target detection with ground penetrating radar using deep learning method," in *2017 25th Signal Processing and Communications Applications Conference (SIU)*. IEEE, 2017, pp. 1–4.

[12] H. Liu, C. Lin, J. Cui, L. Fan, X. Xie, and B. F. Spencer, "Detection and localization of rebar in concrete by deep learning using ground penetrating radar," *Automation in Construction*, vol. 118, p. 103279, 2020.

[13] M. M. Omwenga, D. Wu, Y. Liang, L. Yang, D. Huston, and T. Xia, "Cognitive gpr for subsurface object detection based on deep reinforcement learning," *IEEE Internet of Things Journal*, vol. 8, no. 14, pp. 11 594–11 606, 2021.

[14] Z. Liu, X. Gu, W. Wu, X. Zou, Q. Dong, and L. Wang, "Gpr-based detection of internal cracks in asphalt pavement: A combination method of deepaugment data and object detection," *Measurement*, vol. 197, p. 111281, 2022.

[15] K. A. Colwell, P. A. Torrione, K. D. Morton Jr, and L. M. Collins, "Improving buried threat detection in ground-penetrating radar with transfer learning and metadata analysis," in *Detection and Sensing of Mines, Explosive Objects, and Obscured Targets XX*, vol. 9454. SPIE, 2015, pp. 476–484.

[16] E. Aydin and S. E. Y. Erdem, "Transfer and multitask learning using convolutional neural networks for buried wire detection from ground penetrating radar data," in *Detection and Sensing of Mines, Explosive Objects, and Obscured Targets XXIV*, vol. 11012. SPIE, 2019, pp. 259–270.

[17] M. Garcia-Fernandez, Y. Á. López, and F. L.-H. Andrés, "Airborne multi-channel ground penetrating radar for improvised explosive devices and landmine detection," *IEEE Access*, vol. 8, pp. 165 927–165 943, 2020.

[18] C. Roussi, I. Xique, J. Burns, and B. Hart, "Buried object imaging using a small uas-based gpr," in *Detection and Sensing of Mines, Explosive Objects, and Obscured Targets XXIV*, vol. 11012. SPIE, 2019, pp. 146–154.

[19] J. Zheng, X. Teng, J. Liu, and X. Qiao, "Convolutional neural networks for water content classification and prediction with ground penetrating radar," *IEEE Access*, vol. 7, pp. 185 385–185 392, 2019.

[20] V. J. V. Ylaya, O. J. L. Gerasta, J. M. S. Macasero, D. P. Pongcol, N. M. Pandian, and R. R. P. Vicerra, "Linear frequency modulated continuous wave lfm-cw short-range radar for detecting subsurface water content with deep learning," in *2020 IEEE 12th International Conference on Humanoid, Nanotechnology, Information Technology, Communication and Control, Environment, and Management (HNICEM)*. IEEE, 2020, pp. 1–6.

[21] M. Malajner, D. Gleich, and P. Planinsic, "Soil type characterization for moisture estimation using machine learning and uwb-time of flight measurements," *Measurement*, vol. 146, pp. 537–543, 2019.

[22] J. Liang, X. Liu, and K. Liao, "Soil moisture retrieval using uwb echoes via fuzzy logic and machine learning," *IEEE Internet of Things Journal*, vol. 5, no. 5, pp. 3344–3352, 2017.

[23] K. Muzalevskiy, S. Fomin, and A. Karavayskiy, "Optimum frequency range for remote sensing of soil moisture with various texture, density and organic matter content," in *2022 IEEE International Multi-Conference on Engineering, Computer and Information Sciences (SIBIRCON)*. IEEE, 2022, pp. 1130–1133.

[24] X. Liu, L. Guo, X. Cui, J. R. Butnor, E. W. Boyer, D. Yang, J. Chen, and B. Fan, "An automatic processing framework for in situ determination of ecohydrological root water content by ground-penetrating radar," *IEEE Transactions on Geoscience and Remote Sensing*, vol. 60, pp. 1–15, 2021.

[25] X. Liu, J. Chen, J. Butnor, G. Qin, X. Cui, B. Fan, H. Lin, and L. Guo, "Noninvasive 2d and 3d mapping of root zone soil moisture through the detection of coarse roots with ground-penetrating radar," *Water Resources Research*, vol. 56, no. 5, p. e2019WR026930, 2020.

[26] A. Melebari, M. S. Haynes, S. Prager, Y. Fang, and M. Moghaddam, "Retrieval of soil moisture profile above water table using scattered wave signal structure," in *IGARSS 2022-2022 IEEE International Geoscience and Remote Sensing Symposium*. IEEE, 2022, pp. 2099–2102.

[27] K. Bakian-Dogaheh, R. H. Chen, Y. Yi, J. S. Kimball, M. Moghaddam, and A. Tabatabaeenejad, "A model to characterize soil moisture and organic matter profiles in the permafrost active layer in support of radar remote sensing in alaskan arctic tundra," *Environmental Research Letters*, vol. 17, no. 2, p. 025011, 2022.

[28] C. Oden, G. Olhoeft, D. Wright, and M. Powers, "Measuring the electrical properties of soil using a calibrated ground-coupled gpr system," *Vadose Zone Journal*, vol. 7, no. 1, pp. 171–183, 2008.

[29] G. R. Olhoeft, "Electrical, magnetic and geometric properties that determine ground penetrating radar performance," in *Proceedings of GPR*, vol. 98, 1998, pp. 177–182.

[30] E. T. Selig and S. Mansukhani, "Relationship of soil moisture to the dielectric property," *Journal of the Geotechnical Engineering Division*, vol. 101, no. 8, pp. 755–770, 1975.

[31] G. C. Topp, J. Davis, and A. P. Annan, "Electromagnetic determination of soil water content: Measurements in coaxial transmission lines," *Water resources research*, vol. 16, no. 3, pp. 574–582, 1980.

[32] K. Roth, R. Schulin, H. Flühler, and W. Attinger, "Calibration of time domain reflectometry for water content measurement using a composite dielectric approach," *Water resources research*, vol. 26, no. 10, pp. 2267–2273, 1990.

[33] Z. Datsios and P. Mikropoulos, "Characterization of the frequency dependence of the electrical properties of sandy soil with variable grain size and water content," *IEEE Transactions on Dielectrics and Electrical Insulation*, vol. 26, no. 3, pp. 904–912, 2019.

[34] D. A. Noon, "Stepped-frequency radar design and signal processing enhances ground penetrating radar performance," 1996.

[35] C. Schmelzbach, J. Tronicke, and P. Dietrich, "High-resolution water content estimation from surface-based ground-penetrating radar reflection data by impedance inversion," *Water Resources Research*, vol. 48, no. 8, 2012.

[36] O. Shamir, N. Goldshleger, U. Basson, and M. Reshef, "Laboratory measurements of subsurface spatial moisture content by ground-penetrating radar (gpr) diffraction and reflection imaging of agricultural soils," *Remote Sensing*, vol. 10, no. 10, p. 1667, 2018.

[37] A. Benedetto, "Water content evaluation in unsaturated soil using gpr signal analysis in the frequency domain," *Journal of Applied Geophysics*, vol. 71, no. 1, pp. 26–35, 2010.

[38] X. Liu, X. Cui, L. Guo, J. Chen, W. Li, D. Yang, X. Cao, X. Chen, Q. Liu, and H. Lin, "Non-invasive estimation of root zone soil moisture from coarse root reflections in ground-penetrating radar images," *Plant and Soil*, vol. 436, pp. 623–639, 2019.

[39] L. Zhou, D. Yu, Z. Wang, and X. Wang, "Soil water content estimation using high-frequency ground penetrating radar," *Water*, vol. 11, no. 5, p. 1036, 2019.

[40] P. Anbazhagan, M. Bittelli, R. R. Pallepati, and P. Mahajan, "Comparison of soil water content estimation equations using ground penetrating radar," *Journal of Hydrology*, vol. 588, p. 125039, 2020.

[41] T. Ling, W. He, X. jun Liu, S. Zhang, F. Huang, and F. Hua, "Fine grid model for the dielectric characteristics of ground-penetrating radar in mixed media," *Geophysical Prospecting*, vol. 70, 2022.

[42] D. D. Benedetto, F. Montemurro, and M. Diacono, "Mapping an agricultural field experiment by electromagnetic induction and ground penetrating radar to improve soil water content estimation," *Agronomy*, 2019.

[43] G. Gennarelli, I. Catapano, X. Dérobert, and F. Soldovieri, "A ground penetrating radar imaging approach for a heterogeneous subsoil with a vertical permittivity gradient," *IEEE Transactions on Geoscience and Remote Sensing*, vol. 59, no. 7, pp. 5698–5710, 2020.

[44] R. Persico, "Ill-Posedness and nonlinearity," in *Introduction to Ground Penetrating Radar*. Hoboken, NJ: John Wiley & Sons, Inc, May 2014, pp. 96–104.

[45] Z. Li, Z. Zeng, H. Xiong, Q. Lu, B. An, J. Yan, R. Li, L. Xia, H. Wang, and K. Liu, "Study on rapid inversion of soil water content from ground-penetrating radar data based on deep learning," *Remote Sensing*, vol. 15, no. 7, p. 1906, 2023.

[46] Q. Cheng, S. Zhang, X. Chen, H. Cui, Y. Xu, S. Xia, K. Xia, T. Zhou, and X. Zhou, "Inversion of reclaimed soil water content based on a combination of multi-attributes of ground penetrating radar signals," *Journal of Applied Geophysics*, vol. 213, p. 105019, 2023.

[47] A. A. Pramudita, Y. Wahyu, S. Rizal, M. D. Prasetio, A. N. Jati, R. Wulansari, and H. H. Ryanu, "Soil water content estimation with the presence of vegetation using ultra wideband radar-drone," *IEEE Access*, vol. 10, pp. 85 213–85 227, 2022.

[48] F. Ridhia and A. A. Pramudita, "A method for estimating soil water content in the presence of vegetation using fmcw radar," in *2022 11th Electrical Power, Electronics, Communications, Controls and Informatics Seminar (EECCIS)*. IEEE, 2022, pp. 154–159.

[49] R. Persico, "The 2D scattering equations for dielectric targets," in *Introduction to Ground Penetrating Radar*. Hoboken, NJ: John Wiley & Sons, Inc, May 2014, pp. 48–78.

[50] D. Boutte, V. Radzicki, A. Webb, B. Thelan, and J. Burns, "Acoustically/vibrationally enhanced high frequency electromagnetic detector for buried landmines," AKELA INC SANTA BARBARA CAMICHIGAN TECHONOLOGICAL UNIV ANN ARBOR, Tech. Rep., 2017.

[51] [Online]. Available: https://dynamax.com/products/soil-moisture/pr2-multi-depth-soil-moisture-probe

[52] G. James, D. Witten, T. Hastie, and R. Tibshirani, "Resampling methods," in *Springer Texts in Statistics*, ser. Springer texts in statistics. New York, NY: Springer US, 2021, pp. 197–223.